Chapter 6:
Seasonal Variability of CO_2 in India

This chapter illustrates the present studies carried out on the seasonal variation of atmospheric carbon dioxide (CO_2) in both time and frequency domains. The work, with a combination of field spectroscopy and satellite data analysis, presents an explanation for the annual variability of CO_2 in India under the influences of vegetation activity, atmospheric pressure and temperature. The interpretation is made more generalized by developing a climate model based on the vertical redistribution of CO_2.

6.1. Motivation of the Work

The review of the reported results obtained on the annual changes of CO_2 (Section 2.5) put forward some relevant questions. Though the seasonal variation of CO_2 is well known, the actual nature of the fluctuation is not so well defined. The mean variation over a large area may look like almost sinusoidal but the fluctuation over a smaller area is quite irregular. The present work intends to put up a reasonable interpretation of the periodicity through the following steps.

- The trend of the annual periodic variation of atmospheric CO_2 is explored in both time and frequency domains.
- A valid reason for oscillatory variation is suggested in relation to atmospheric pressure.
- A suitable atmospheric model is developed based on vertical redistribution of CO_2 concentration to explain the phenomena.

The study includes several regions of the plain areas of north India having tropical climate. These regions are of varying extents of vegetated area and urban congestion. The seasonal variations of atmospheric CO_2 concentration (ppm) are investigated. The simultaneous variations of the vegetation activities and atmospheric pressure and temperature are also taken into consideration. The studies were carried out at three levels.

(i) Initially the Orbiting Carbon Observatory-2 (OCO-2) data were analysed for the seasonal changes of CO_2 and the corresponding changes of solar-induced fluorescence (SIF), surface pressure and air temperature for a specific region of 1° × 3° (Latitude × Longitude) extension for consecutive years

(ii) The investigations were then generalized with a number of urban places over 9° × 20° (Latitude × Longitude) extension of similar atmospheric conditions using the National Aeronautics and Space Administration (NASA)-Giovanni data on the monthly averages of CO_2 concentration, the corresponding Normalized Difference Vegetation Index (NDVI), the surface pressure and the surface temperature.

(iii) The atmospheric CO_2 concentration in parts per million (ppm) was derived at specific sites from ground-based spectroradiometry.

Based on the above satellite data and ground spectroradiometry, the present work infers about the effect of atmospheric pressure on the annual variability of CO_2 column average and develops a mathematical model based on vertical redistribution of CO_2 molecules for interpreting the results.

6.2. Data and Methodology

The work is based on satellite data analysis on CO_2 concentration and ground measurement of directly incident solar irradiance containing CO_2 absorption bands. The two components are introduced below.

6.2.1. Satellite Data

The following two independent sources of satellite-derived database were used for CO_2 analysis.

(i) Day-wise, column averaged, bias corrected dry air CO_2 mole fraction (xCO_2) retrieved from Orbiting Carbon Observatory 2 (OCO-2) were downloaded from NASA's Goddard Earth Sciences Data and Information Services Center (GES-DISC) (https://disc.gsfc.nasa.gov) for the region bounded by 22° N to 23° N and 86° E to 89° E. This region comprises the sites of ground-based spectroradiometric measurements. It is a plain area having moderate tropical wet-and-dry climate and uniform seasonal variation. The surface vegetation is

about 66% and the land use to land cover ratio is around 4:5. Three other relevant parameters, namely solar-induced chlorophyll fluorescence (SIF), surface pressure and surface temperature of the atmosphere were also extracted for this region.

(ii) The monthly averaged atmospheric CO_2 mole fraction (ppm) and three more parameters, namely *normalized difference vegetation index* (NDVI), surface pressure and surface air temperature data were procured (Table 6.1) from NASA Giovanni online environment geophysical parameter (https://giovanni.gsfc.nasa.gov/giovanni/) for the period of January, 2010 to December, 2017.

Table 6. 1. Specification of parameters downloaded from NASA Giovanni online environment

Parameter	Source	Temporal resolution	Spatial resolution (°)
Carbon dioxide, mole fraction in free troposphere, infrared only	Atmospheric Infrared Sounder Earth Observing System (AIRS EOS) Aqua satellite sensor	Monthly	2.5 × 2.0
NDVI	Moderate Resolution Imaging Spectroradiometer (MODIS)-Terra satellite sensor	Monthly	0.05 × 0.05
Surface air pressure	Global Land Data Assimilation System Version 2 (GLDAS-2) surface observation and model-based re-analysis/ data assimilation system	Monthly	0.25 × 0.25
Surface air temperature	Modern-Era Retrospective analysis for Research and Applications, Version 2 (MERRA-2) surface observation and model-based re-analysis/ data assimilation system	Monthly	0.500 × 0.625

The objective of including the second category of data was to understand the average trend of variation of CO_2 concentration over a large area of similar climate. It contained Kolkata (the place of ground measurement) and twenty-four other urban areas

of India within approximately 20° N to 29° N and 69° E to 89° E (Figure 6.1 and Table 6.2). These places are, as understood from Table 6.2, of similar plain, urban area under similar tropical climatic conditions but differ in the quantity of vegetation and the possible amount of CO_2 emission. This wide choice of regions includes several thermal power plants also.

Table 6. 2. Land use land cover information for the states containing the 25 places of Figure 6.1 for obtaining CO_2 monthly average data (Source: calculated from the statistics of 2015 to 2016 provided by *Bhuvan*, Indian Geo-Platform of Indian Space Research Organization, National Remote Sensing Centre, India (https://bhuvan-app1.nrsc.gov.in/thematic/thematic/index.php).

State	Including Site Nos. of Fig. 6.1	The extents of geographic features (%)				
		Agriculture	Barren	Built up	Forrest/Grass	Waterbody/ Wetland/ Snow
Bihar	16	77.29	2.87	6.98	6.26	6.60
Chhattisgarh	4, 17, 23	45.74	2.71	3.31	45.70	2.54
Delhi	5	34.66	5.09	57.36	1.00	1.89
Gujarat	1, 11, 20, 21	62.06	21.56	2.84	6.72	6.82
Jharkhand	6, 12	50.01	7.08	5.72	34.60	2.59
Madhya Pradesh	2, 7, 8, 19, 25	61.04	8.06	1.86	26.15	2.89
Odisha	3, 18, 24	50.85	7.19	4.16	33.14	4.66
Rajasthan	9	67.96	19.13	1.70	9.28	1.93
Uttar Pradesh	14, 15, 22	80.73	3.09	5.31	6.48	4.39
West Bengal	10, 13	61.04	1.32	18.08	11.27	8.29

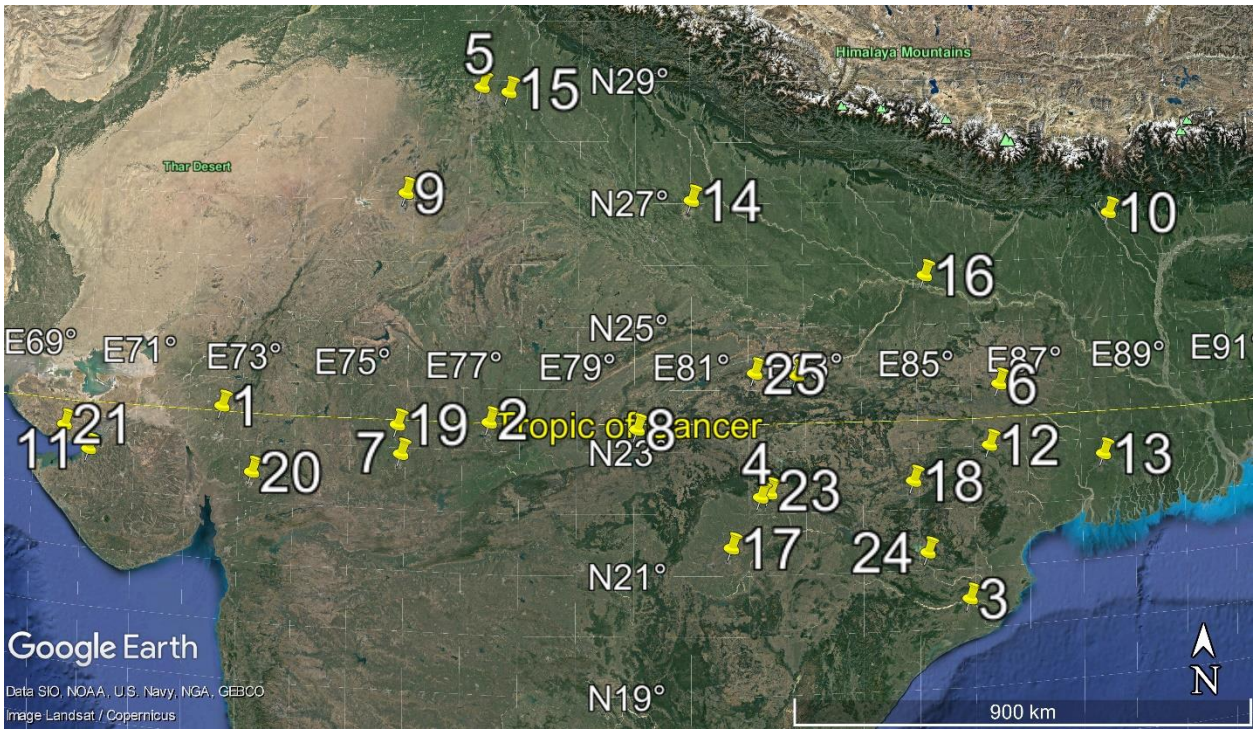

Figure 6. 1. Twenty-five urban places of India in relation to section 6.2.1 for procuring CO_2 monthly average data from NASA- Giovanni online environment. The sites are: 1. Ahmedabad, 2. Bhopal, 3. Bhubaneswar, 4. Bilaspur, 5. Delhi, 6. Dhanbad, 7. Indore, 8. Jabalpur, 9. Jaipur. 10. Jalpaiguri, 11. Jamnagar, 12. Jamshedpur, 13. Kolkata, 14. Lucknow, 15. NTPC Dadri, 16. Patna, 17. Raipur, 18. Rourkela, 19. Ujjain, 20. Vadodara and thermal power stations of 21. Mundra, 22. Rihand, 23. Sipat, 24. Talcher, 25. Vindhyachal.

The temporal variation of CO_2 was fitted linearly and the estimated linear increment was subtracted from each data. Thus only the seasonal fluctuation component superposed to the initial value was retained. The temporal change of the other three parameters, namely NDVI, surface air pressure and surface air temperature for the same regions were considered directly. The following are the justifications for taking these parameters into account.

(i) The NDVI is expected to be an indicator of CO_2 absorption by vegetation through the process of photosynthesis (Gamon et al., 1995; Nestola et al., 2016).

(ii) The SIF originates only from the plant pigment chlorophyll, which is directly associated with CO_2 removal by photosynthesis whereas the NDVI includes

the overall influence of other leaf tissues and canopy structure. Although this cannot be correlated directly with CO_2 elimination, it indicates a healthy vegetation, an indirect indication of CO_2 uptake.

(iii) The possible role of atmospheric pressure and temperature in the seasonal variation of CO_2 can be anticipated from the review of section 2.5.

6.2.2. Ground Measurements

The objective of this experimental study was to find out the possible relationship between the column-averaged CO_2 concentration (ppm) with the concentration (ppm) at surface level. The following two types of measurements were carried out simultaneously.

(A) Solar Irradiance Spectra: The solar spectral irradiance were measured with Analytical Spectral Devices (ASD) spectroradiometer with the following specifications.

- Sites: different places of Kolkata city (around 22.55° N, 88.35° E)
- Ambient condition: cloud-free solar illumination
- Spectral range: ultraviolet-visible-shortwave infrared, 350 to 2500 nm
- Spectral resolution: spectral sampling interval of 1.4 nm for 350 to 1000 nm and 2 nm for 1000 to 2500 nm.

The instrument was held vertically upward and was fitted with wide angle (Field of View 180°) remote cosine receptor on the fiber of 25° Field of View.

(B) Local CO_2 Concentration: At the same time, the local concentrations (ppm) of atmospheric CO_2 at the ground level were measured with handheld carbon dioxide meter Model GCH-2018.

The above measurements were conducted through urban places of widely varying population and vehicle congestion. Two consecutive CO_2 absorption bands around 2 μm, introduced earlier as CO_2-1 and CO_2-2, respectively were identified on the irradiance spectra and the CO_2 concentrations (ppm) were estimated from the absorption depths

using the differential optical absorption spectroscopic (DOAS) technique mentioned in section 2.4.

6.3. CO_2 Redistribution Model

This section illustrates a simple mathematical model developed for explaining the change of CO_2 concentration at an arbitrary atmospheric height with respect to that at ground level caused by change in atmospheric temperature, hence in atmospheric pressure. As known from literature (Sawyer 1972; Berner 2003; Queißer et al. 2019), the net atmospheric CO_2 is the outcome of the following simultaneous contributions.

- The major sources, namely human activities, volcanic explosion and biosphere respiration.
- The major sinks, such as vegetation, ocean and soil.
- The complex feedback from organic matter.

The majority of the above entities exist on the earth surface and the vertical diffusion of the surface emitted CO_2 slowly changes the average air-mixed amount of it over the whole atmospheric column. Since CO_2 is chemically less reactive, it persists in the atmosphere for a long time and both its sequestration to sinks and mixing with air are very slow processes. Therefore, the total number density $N(z)$ of atmospheric CO_2 molecules present at an arbitrary altitude z at a certain instant of time is being expressed as a sum of two components:

$$N(z) = n(z) + \upsilon(z) \tag{6.1}$$

In Eq. (6.1), $n(z)$ represents the number density of CO_2 molecules that are well-mixed with air and are governed by the instantaneous atmospheric temperature and pressure. In contrast, $\upsilon(z)$ denotes the randomly varying net amount of CO_2 molecules resulting from the supply from the sources and the assimilation by the sinks. This second component is (i) not blended uniformly in the air, (ii) does not obey the instantaneous air pressure and temperature and (iii) accounts for the random vertical change of CO_2

concentration because of the gradual diffusion of surface-level air throughout the atmospheric altitude.

Assuming the ideal gas law to be valid for air, the rate of change of the partial pressure (P) of CO_2 with height (z) is expressed as

$$\frac{\mathrm{d}P}{\mathrm{d}z} = -\chi\rho_0 g \tag{6.2}$$

In Eq. (6.2), the equilibrium density of CO_2 is given by $\rho_0 = (P \times M)/(R_G \times T)$ is, the acceleration due to gravity is g = 9.8 m s^{-2}, the molecular weight of CO_2 is M = 44 × 10^{-3} kg mol^{-1} is, the gas constant is R_G = 8.31 J K^{-1} mol^{-1}, the atmospheric temperature (K) is T and χ is a dimensionless constant accounting for the fluctuation in the vertical density profile. When χ becomes unity, the ideal condition of the rate of change of pressure with altitude is obtained. A smaller value of χ corresponds to a sharper change of pressure with altitude. The number density of CO_2 depending on the altitude (hence on the pressure) can be expressed as $n(z) = (A \times P)/(R_G \times T)$ where A = 6.023×10^{23} molecules mol^{-1} is the Avogadro number. Using Equation (6.2) and the related expressions, one can obtain the rate of change in $n(z)$ at an arbitrary temperature as

$$\frac{\mathrm{d}n(z)}{n(z)} = -\chi\left(\frac{gM}{R_G T}\right)\mathrm{d}z, \tag{6.3}$$

Eq. (6.3) can be integrated over the altitude for obtaining the number density of CO_2 molecules as function of altitude. The standard linear decrease of atmospheric temperature (T) with altitude within the troposphere (Elachi and van Zyl 2006) is implemented as $T = T_0 - \alpha \times z$, T_0 being the equilibrium surface temperature and α is a constant lapse rate (K m^{-1}). Then the integral is obtained as

$$n(z) = n_0\left(1 - \frac{\alpha z}{T_0}\right)^k \tag{6.4}$$

Eq. (6.4) represents the pressure dependent number density of air-mixed CO_2 at an arbitrary altitude z, the number density at ground level being given by n_0 and

$$k = \left(\frac{\chi g M}{\alpha R_G} \right) \tag{6.5}$$

is a dimensionless constant quantity accounting for the maximum attainable altitude for the trace gas. At a certain maximum altitude, the number of CO_2 molecules becomes almost zero so that the term $\left(1 - \frac{\alpha z}{T_0}\right)$ in Equation (6.4) becomes almost zero implying z becomes almost T_0/α. For instance, assuming T_0 = 300 K and α = 0.0065 K m^{-1}, z is about 45 km. The generality of Equation (6.4) can be verified in the following way. It is apparent from the aforementioned standard values of parameters that $k >> 1$. Assuming $k \rightarrow \infty$ and using the identity $\lim_{k\to\infty}(1 + x/k)^k \rightarrow \exp(x)$, Equation (6.4) can be approximated as

$$n(z) = n_0 \exp\left(-\frac{\chi z}{H} \right) \tag{6.6}$$

Eq. (6.6) represents the ideal case of exponential decrease of atmospheric gaseous molecular density with altitude (Elachi and van Zyl 2006) where $H = (R_G \times T_0)/(g \times M)$ = 5.78 km can be designated as the *scale height* for CO_2. Furthermore, $n(z)$ represents the number of CO_2 molecules per unit volume of air and is proportional to its mole fraction [$xCO_{2(z)}$] at altitude z. Accordingly Equation (6.4) can be further reformed in terms of the mole fraction as

$$xCO_{2(z)} = xCO_{2(0)} \exp\left(-\frac{\chi z}{H} \right) \tag{6.7}$$

where $xCO_{2(0)}$ is the mole fraction at ground surface. Eqs. (6.6) and (6.7) demonstrate the general validity of Eq. (6.4). The present work considers Eq. (6.4) in its original form.

The $\upsilon(z)$ component in Eq. (6.1) represents the net unmixed CO_2 suspended in air at an altitude z. This CO_2 outcome results from the source-sink interaction and the vertical transport by random diffusion process. The dispersion of atmospheric particles due to wind and eddy motion can be expressed as Gaussian function of altitude (Stockie 2011). Therefore, $\upsilon(z)$ can be quantified by Gaussian variation over the altitude as

$$\upsilon(z) = \upsilon_h \exp\left[-\frac{(z-h)^2}{\sigma^2}\right] \tag{6.8}$$

In Eq. (6.8), υ_h represents the instantaneous unmixed CO_2 concentration at arbitrary height h ($0 < h < z$) under the average effect of wind advection and σ accounts for the standard deviation of the distribution in Gaussian concentration resulting from the eddy variation over the atmospheric altitude. The scope for reflection of CO_2 from the ground surface is assumed to be negligible in comparison with the above. The υ_h part of CO_2 is expected to possess the following two features.

(i) It undergoes slow change, hence it remains unchanged for a certain instant of time.

(ii) It remains well below the aforementioned upper limit of altitude because of two reasons. There is negligible source of CO_2 above the troposphere and there is low mixing ratio above 15 to 20 km with strong gradients across the tropopause (Diallo et al., 2017).

Now considering the above two components of CO_2 molecules, namely $n(z)$ and $\upsilon(z)$, the effect of temperature and pressure on the vertical distribution of CO_2 molecules over an atmospheric column can be interpreted.

Let n_1 and n_2 be the number densities of CO_2 molecules at the same atmospheric altitude (z) for two different surface temperatures T_{01} and T_{02} and n_{01} and n_{02} be the corresponding ground level number densities. The CO_2 column reaches up to the height of z_1 when the ground level temperature is T_{01}. If this temperature is increased to T_{02}, the same number of CO_2 molecules attains an increased height of z_2 due to decrease in pressure and consequent expansion. The lateral expansion is neglected assuming the immediate neighbouring places to be at the same temperature. The integrals of Eq. (6.1) over these two different altitudes should be equal because only the vertical distribution gets changed but the total number of CO_2 molecules reaching two different heights (z_1

and z_2) at two different surface temperatures (T_{01} and T_{02}, respectively) must remain the same. Therefore,

$$\int_0^{z_1}(n_1+\upsilon)\mathrm{d}z=\int_0^{z_2}(n_2+\upsilon)\mathrm{d}z \tag{6.9}$$

As mentioned earlier, the action of $\upsilon(z)$ is slow and it remains well below the upper limit of CO_2 column. Therefore, its integrated effect over the altitudes z_1 and z_2 remains the same for both sides of Eq. (6.9) and is cancelled out. Thus, on integrating the two sides of Eq. (6.9) and equating the results, one can obtain

$$n_{02}=n_{01}\left(\frac{T_{01}}{T_{02}}\right)\frac{1-\left(1-\frac{\alpha z_1}{T_{01}}\right)^{k+1}}{1-\left(1-\frac{\alpha z_2}{T_{02}}\right)^{k+1}} \tag{6.10}$$

Eq. (6.10) defines the changed number density (n_{02}) at ground surface due to change in temperature in terms of the parameters of Eq. (6.4). The above combinations of Equations (6.1), (6.4), (6.8) and (6.10) considered altogether put up the concept that the seasonal change in surface air temperature can cause a change in air pressure. The consequent expansion or contraction of air can give rise to a change in elevation and redistribution of the surface level CO_2 molecules resulting in an apparent change in the gas concentration at any specific height (z) of the atmosphere. When the $\left(1-\frac{\alpha z}{T_0}\right)$ terms in Eq. (6.10) approximate to zero similar to the case of Eq. (4), the expression for the changed number density can be simplified as

$$n_{02}=n_{01}\left(\frac{T_{01}}{T_{02}}\right) \tag{6.11}$$

Using Equations (6.10) and (6.11), the corresponding increased height can be related to the initial height as

$$z_2 = z_1\left(\frac{T_{02}}{T_{01}}\right) \tag{6.12}$$

It is understood from Equations (6.11) and (6.12) that the redistribution may elongate the atmospheric path of radiation propagation through the CO_2 molecules in comparison with that at lower temperature so that the possibility of undergoing more radiation absorption is enhanced. It yields an apparently higher value of concentration at higher temperature.

6.3.1. Parameter Assessment in Redistribution

The relevant parameters used in the above equations are estimated in the following ways. The CO_2 column average concentration at Kolkata obtained from OCO-2 data for the date of the ground measurements was considered as the preliminary reference. The altitude profile of tropical atmospheric pressure was simulated with MODTRAN6 software and the slope was determined near the surface. The magnitudes of the slope (5.88 to 11.76 Pa m^{-1}) were used in Eq. (6.2) assuming it to be valid for air also with the corresponding values of pressure and density. For air density = 1.2 kg m^{-3} and g = 9.8 m s^{-2}, the value of χ came out to be around 0.7. Therefore, the possible numerical values of χ in Eqs. (6.5) and (6.10) varied from 0.5 to 1.0. The temperature values for Equations (6.11) and (6.12) were obtained from the open source website: https://www.timeanddate.com/weather/india/kolkata/climate. The given temperature values being given in Celsius were converted to the absolute (K) values and the mean of the maximum and minimum temperatures of each concerned day was used in the calculation.

6.3.2. Validation of the Model

The above model was justified with respect to the annual variability of CO_2 using the monthly average values of surface temperature in India downloaded from the open data archival of Indian Institute of Tropical Meteorology (https://www.tropmet.res.in/) for years 2000 to 2016. The values averaged for each month were fitted with third order polynomial to regress a continuous daily temperature variation throughout a year. The vertical CO_2 profile was generated with the model described above for each day using the corresponding temperature value. The total CO_2 (ppm) throughout the column was summed up and the percentage of increase/decrease with respect to the minimum was assessed. That accounted for the effect of seasonal variability of temperature, hence that of pressure. In actuality, the seasonal CO_2 variation assessed from OCO-2 or other similar spectroscopic technique gets influenced by at least two more entities, as given below.

(i) The occurrence of the monotonic increase throughout the year due to the mixing of the surface-emitted CO_2 in the air column was simulated by adding a linear term [proportional to (1/365) × day] to Equation (6.1).

(ii) The sequestration caused by vegetation activity having random variation with growth, senescence and deciduous properties and having a seasonal fluctuation was replicated by subtracting a Gaussian term proportional to exp[– (day – 250)^2/3650] with peak in autumn days from Equation (6.1).

6.4. Results and Discussion

6.4.1. CO_2 Trend and Effect of Vegetation

The annual variations of CO_2 at the specified region are displayed in Figure 6.2 for years 2017 and 2018 when sufficient data throughout the year were available. The winter season for the local climate is spanned by the two ends of the year, the months of January and December. The middle portion (April-June) represents mainly the summer season and the commencement of monsoon. As pointed out in section 6.1, the actual trend of the annual variability should be defined quantitatively. The same effort is exerted with these plots.

Each point of the graph corresponds to a different day and represents an independent information. Therefore, to comprehend the seasonal variation, the plotted points were fitted with second to fifth order polynomials. The third order polynomial made prominent three distinct features, namely the increase in summer, the decrease in autumn and the tendency of increase in the next winter. No further significant changes in the features were found on increasing the polynomial order. Therefore, all the data points were fitted with third order polynomial, as represented in Figure 6.2. The tendency of increasing the CO_2 concentration in summer season is obtained prominently in the plots, which is in compliance with some previous reports (e.g. Basu et al., 2014) but contrary to some others (e.g., Keeling et al. 1996). Also, the curves show a tendency to increase the concentration at the end of the year.

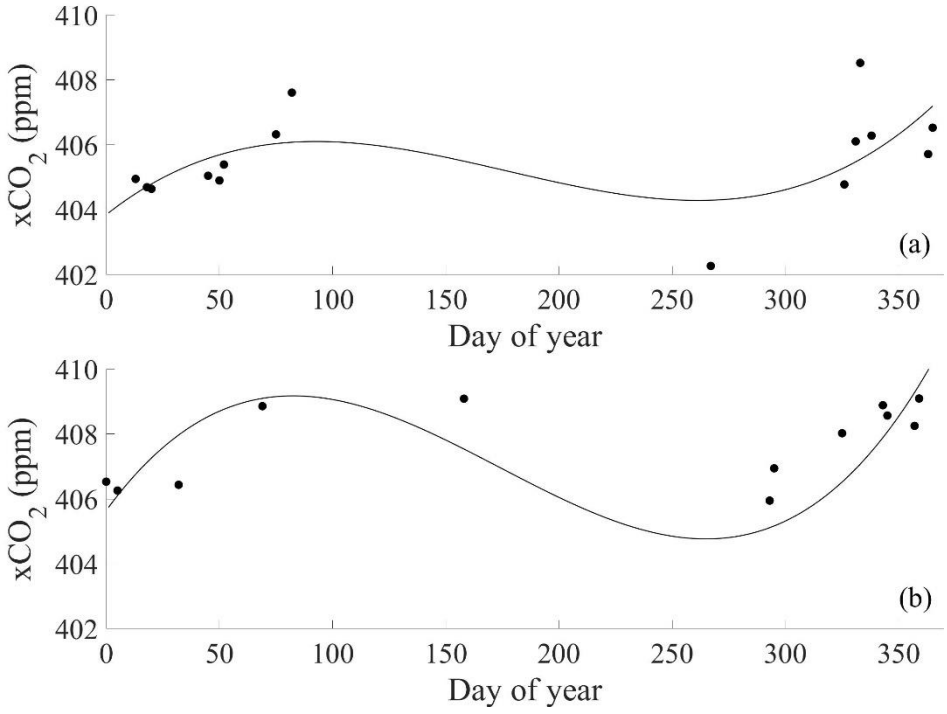

Figure 6. 2. xCO_2 (ppm) variation throughout the year for (a) 2017, (b) 2018 retrieved from OCO-2 database for coordinate range 22° N to 23° N and 86° E to 89° E.

The above nature of the annual CO_2 variation is cross-checked in Figure 6.3, which plots the CO_2 data obtained from AIRS, an independent source, for the region covered in Figure 6.2. It is noted that in most cases, the annual CO_2 change fitted with third order polynomial exhibits an increase in summer. These findings approve that the seasonal variation of CO_2 with an increment in summer is a characteristic feature of this region irrespective of the time of observation and the sensor for detection.

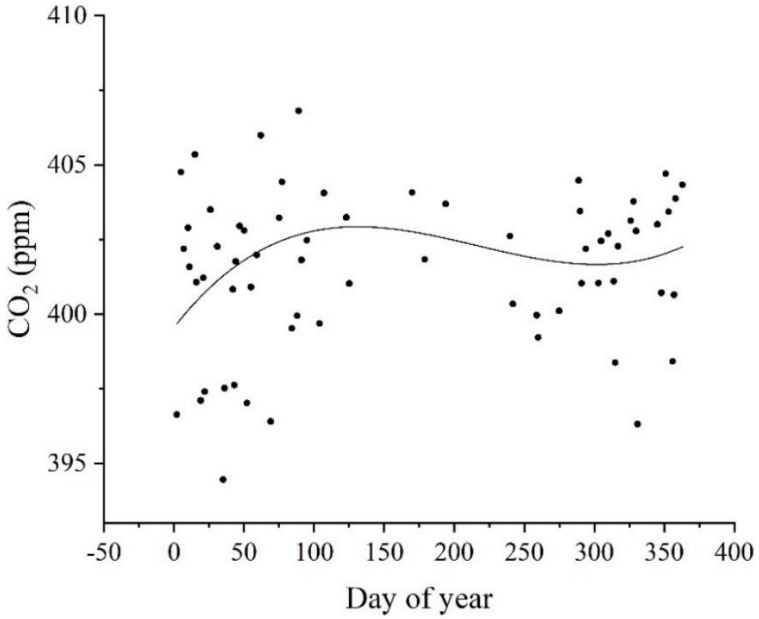

Figure 6. 3. Annual CO_2 (ppm) variation for the year 2016 extracted from AIRS database for the region 22° N to 23° N and 86° E to 89° E.

In continuation of the above findings, the role of photosynthesis in vegetation in connection with CO_2 sequestration is explored with Figure 6.4, which displays the seasonal variations of solar-induced chlorophyll fluorescence (SIF) obtained from the OCO-2 database for the same region and period as that of Figure 6.2. At the first glance, the seasonal trend of SIF appears to be the 'mirror image' of that of CO_2. The higher SIF period corresponds to the time span of lower CO_2. However, the extent of SIF has remained almost the same during the two years whereas the range of CO_2 data points has varied significantly during this time. Table 6.3 compares the present results with a

previously reported result (Basu at al., 2014) where the seasonal CO_2 variation is found not to synchronize with that of SIF. This implies that though the vegetation vigour indicated through SIF is a key reason for CO_2 sequestration, the present finding about the seasonal variation of SIF is not in full conformity with the seasonal change of CO_2 concentration over the atmospheric column. It is realized that further investigation is needed to interpret the annual CO_2 change.

Table 6. 3. Comparison of CO_2 abundance and fluorescence response

Reference	Data source	Area	Period	Approximate seasonal variations	
				CO_2 (ppm)	Fluorescence ($Wm^{-2}\,sr^{-1}\,\mu m^{-1}$)
Basu et al. 2014	GOSAT, CONTRAIL	Tropical Asia 10° S to 28° N and 80° E to 156° E	January 2009 to September 2011	385 to 393 Max: May Min: September	0.2 to 0.5 Max: July-August Min: December-January
Present work	OCO-2, AIRS and NASA-Giovanni	Tropical urban areas (i) 22° to 23° N and 86° to 89° E (ii) 20° to 29° N and 69° to 89° E approx.	(i) January 2017 to December 2018 (ii) January 2010 to December 2017	395 to 415 Max: April-May Min: August-October	0.2 to 1.0 approx. Max: August-October Min: February-March and December

Abbreviations:
GOSAT: Greenhouse Gases Observing Satellite
CONTRAIL: Comprehensive Observation Network for Trace gases by Airliner

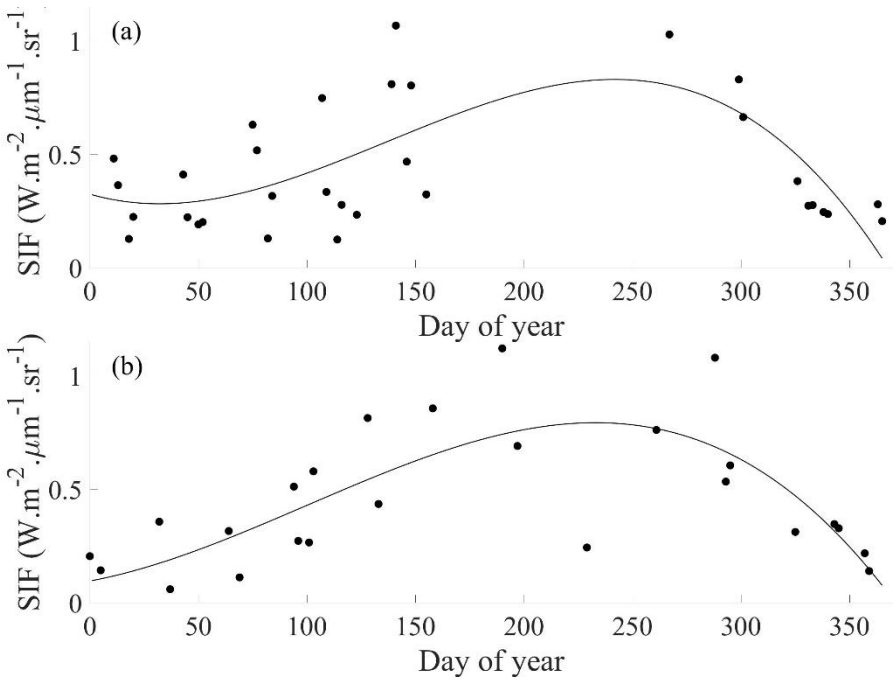

Figure 6. 4. Annual fluctuation of solar induced fluorescence (Wm–2m–1sr–1) retrieved from the OCO-2 database for the years (a) 2017 and (b) 2018 for the area between 22° N and 23° N and 86° E and 89° E.

6.4.2. The Role of Atmospheric Pressure

The comparative study of the CO_2 seasonal variation and the corresponding variation of vegetation vigour presented above indicate that it is not just enough to correlating the seasonal growth of terrestrial vegetation to CO_2 uptake and the subtle influence of some other parameters need to be identified. Several factors related to the seasonal change of CO_2, such as nonuniform warming of the atmosphere, wind direction, climatic variability and surface temperature are mentioned in the review of section 2.4. These all entities are somehow related to a common factor that is the atmospheric pressure. Therefore, the effect of atmospheric pressure was investigated, first at local scale and then over an extended region.

Figure 6.5 represents the seasonal change of the atmospheric surface pressure extracted from OCO-2 database for the region and period mentioned same as those of Figure 6.2. The corresponding air temperatures obtained from the same data source are also given for comparison. It is apparent from Figure 6.5 that the surface pressure

decreases in monsoon and autumn seasons and increases in the winter (two ends of the year). The opposite trend is shown by the surface air temperature in conformity with the fundamental inverse relationship between pressure and temperature.

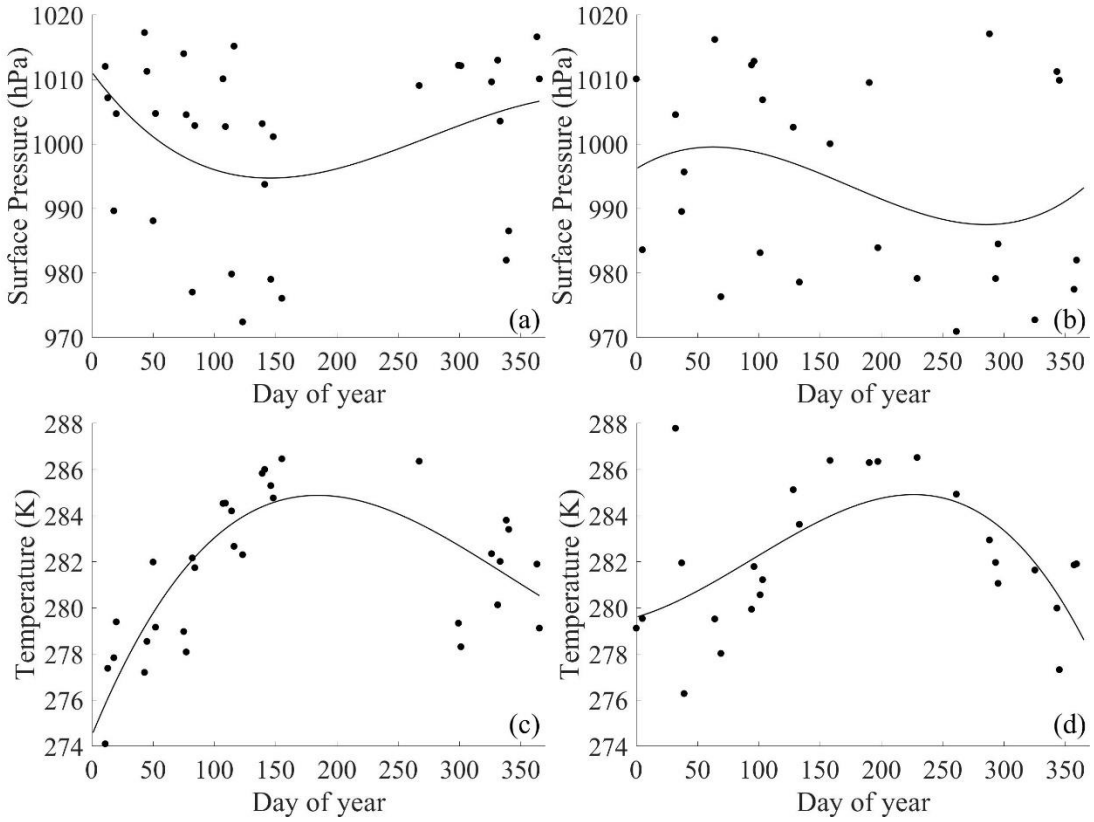

Figure 6. 5. For the years 2017 and 2018, annual variations in (a) and (b)surface pressure (hPa) and (c) and (d) air temperature (K) were taken from the OCO-2 database for the area between 22° N and 23° N and 86° E and 89° E.

The trend of seasonal variation of surface pressure does not match that of CO_2 but it is noteworthy that the lowered CO_2 in the winter at the beginning of the year matches the higher surface pressure and up to the summer, these two entities exhibit the opposite tendency. The pressure decreases while the CO_2 increases; as if the lowering of pressure supports the enhancement of CO_2. Thus, a strong influence of atmospheric pressure on the seasonal variation of CO_2 concentration is indicated, which is studied for a longer period in the next section.

6.4.3. Long-Term Variation of Parameters

In order to get more comprehensive idea on the generalized trends of seasonal changes, the long duration changes of the parameters mentioned in the previous section were investigated over an extended area indicated in Figure 6.1. The study on the temporal change was initiated with four randomly chosen sites from those of Figure 6.1. The monthly CO_2 variation for these sites are shown in Figure 6.6. It is noted that each one exhibits a steady increase with time, an irregular annual fluctuation being superimposed.

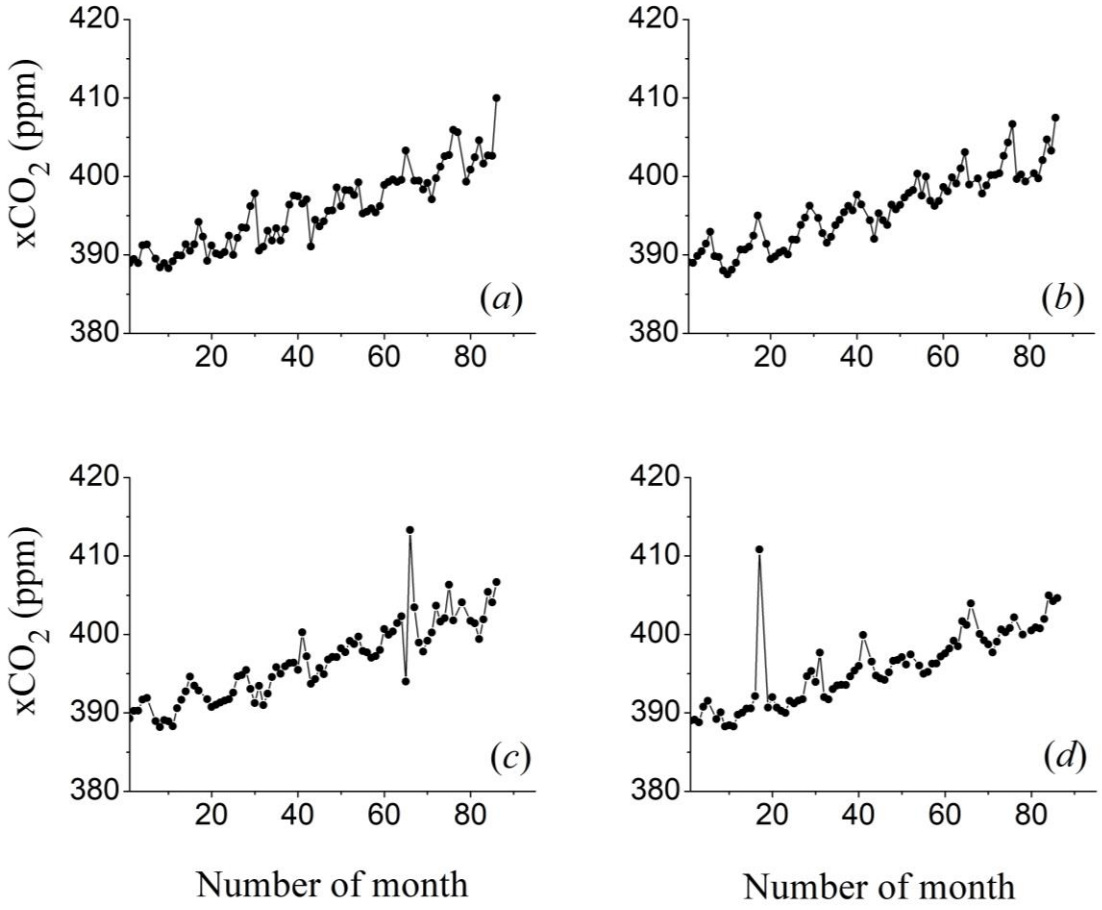

Figure 6. 6. Annual variation of CO_2 concentration over the period of year 2010 to 2017 for four randomly selected places of Figure 1, namely (*a*) Ahmedabad (No. 1), (*b*) Bhopal (No. 2), (*c*) Delhi (No. 5) and (*d*) Rourkela (No. 18), obtained from NASA-Giovanni database specified in Table 6.1.

The picture is made more illustrative by averaging the CO_2 concentration values for all the twenty-five places for each month, as plotted in Figure 6.7(*a*). Comparing with the plots of Figure 6.6, it is quite apparent that the annual periodicity in Figure 6.7(*a*) has become more prominent and organized. It remains no longer any irregular waveform but exhibits a clear positive trend of increment superimposed by a uniform seasonal cycle. This comparison of figures 6.6 and 6.7(*a*) demonstrates how the global CO_2 variation averaged over a vast area assumes a well-defined periodicity. This is the reason why we observe the global change of CO_2 with a well-shaped periodicity.

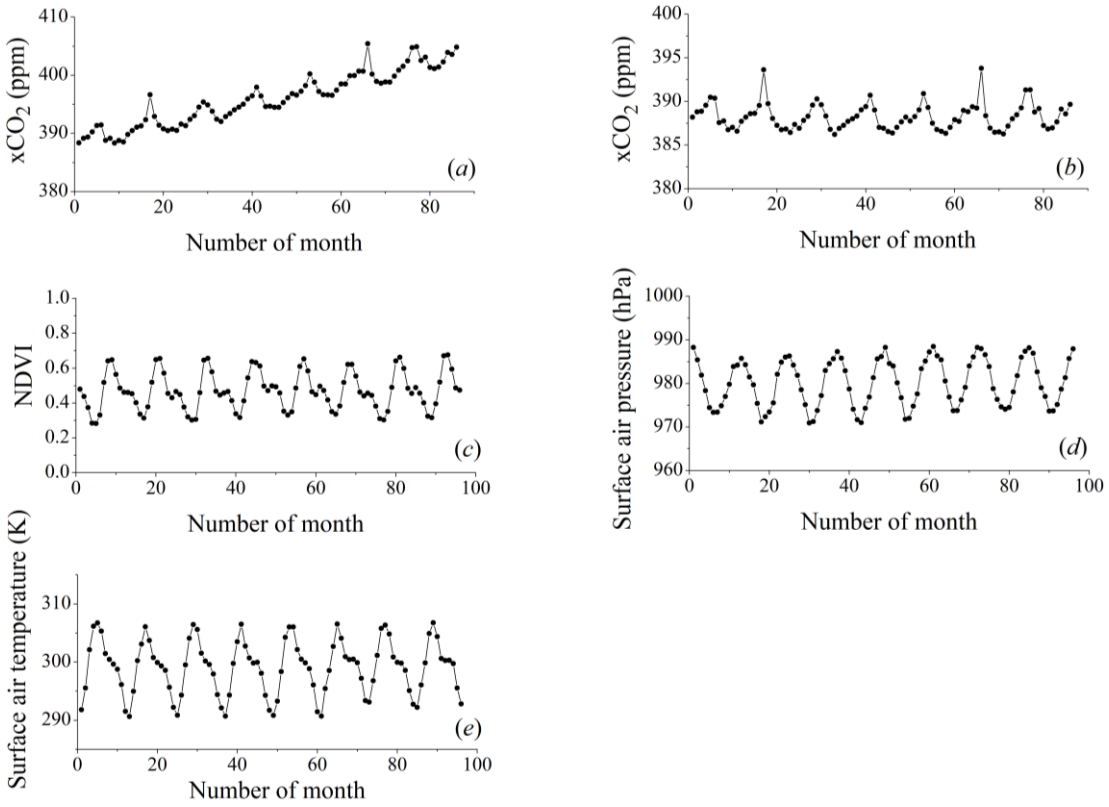

Figure 6. 7. Annual variation of (*a*) CO_2 concentration, (*b*) seasonal fluctuation over the initial value of CO_2 concentration, (*c*) NDVI, (*d*) surface pressure and (*e*) surface air temperature for the period of year 2010 to 2017, each parameter averaged over the twenty-five urban areas of Figure 6.1, obtained from NASA-Giovanni database specified in Table 6.1.

Figure 6.7(*b*) shows only the seasonal fluctuation component of the temporal variation of CO_2, isolated by subtracting the fitted linear increment from each data value. The corresponding seasonal variations of NDVI values, varying widely for the above sites were averaged, as plotted in Figure 6.7(*c*). It is apparent from figures 6.7(*b*) and 6.7(*c*) that the CO_2 and the NDVI have almost inverse relationship. The CO_2 has a tendency to increase when the NDVI decreases and vice versa.

The next parameters under the study were the trend of variation of atmospheric pressure and temperature for the above regions. The monthly values of surface pressure averaged over the sites are plotted in Figure 6.7(*d*) and the corresponding surface air temperature values are given in Figure 6.7(*e*). It is quite noticeable that the pressure and the temperature undergo changes in opposite phase.

Comparing the findings of figures 6.7 (*b*), (*d*) and (*e*) it comes out that annual variation of the atmospheric pressure due to change in temperature is in consort with the annual change of CO_2. At the same time, the results obtained with figures 6.7(*b*), 5(*c*) and 5(*d*) imply that the NDVI minima almost coincides with the CO_2 maxima and the air pressure minima have a phase shift of few months with the CO_2 maxima. Thus, the NDVI and the atmospheric pressure have a combined influence on the seasonal variation of CO_2 concentration. It periodicities of all the temporal variations are quite prominent but none of the parameters has any regular waveform. Also it appears from the plots that the variations consist of more than one periodic component. In order to discover their individual roles, the frequency-domain analysis of the above time variations were conducted, as illustrated in the next section.

6.4.4. Fourier Transform Analysis

The net outcome of Figure 6.7 is that the seasonal variations of both the NDVI and the atmospheric pressure are somehow related to the seasonal change of atmospheric CO_2 but none of these alone can explain the phenomena. The increasing phase of NDVI does not synchronize with the decreasing phase of CO_2 indicating that the vegetation sequestering cannot be correlated directly with the period of carbon uptake. Similarly the annual

increase and decrease of the atmospheric pressure at the surface does not coincide with that of CO_2. A phase difference of several months exists between them. The actual role of these parameters can be explored more precisely with Figure 6.8 that depicts the Fourier transforms for the temporal variations of CO_2, NDVI and air pressure corresponding to those given in Figure 6.7.

Figure 6.8 reveals that the CO_2 variation displays two periodicities, a pronounced annual change and a feeble semi-annual whereas the NDVI exhibits both annual and semi-annual periodicities almost equally prominent. The atmospheric pressure, in contrast, shows a single periodicity that is the annual one. The findings from figures 6.7 and 6.8 infer that the CO_2-NDVI relationship, as expected, is anti-phase for both annual and semi-annual variations and consequently the increase of one parameter corresponds to the decrease of the other. The CO_2-Pressure interaction is, howbeit, of a different nature. It influences mainly the annual variation and partly the semi-annual variation. In both cases, there exists a phase difference between these two. If only the annual variation is considered, the effect of surface pressure is found to be more systematized than that of NDVI.

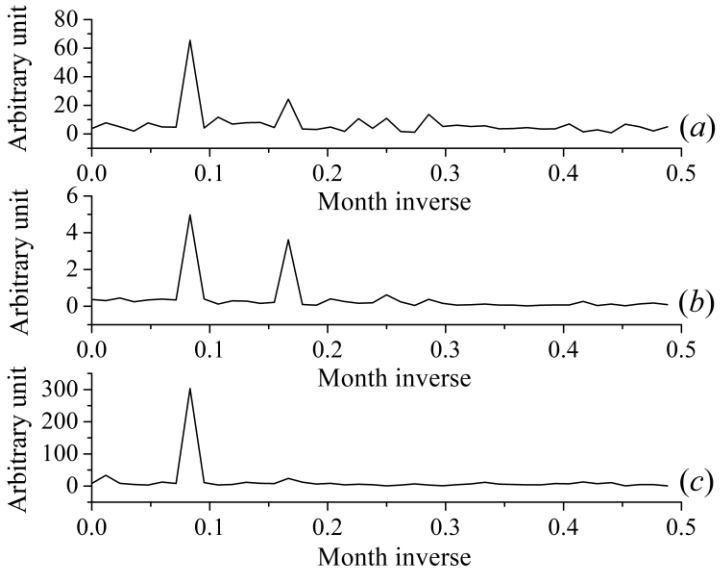

Figure 6. 8. Fourier transform spectra for (*a*) CO_2, (*b*) NDVI and (*c*) surface pressure for the regions specified with Figure 6.7. The arbitrary units indicate the proportional variations of the parameters.

6.4.5. Vertical Redistribution of CO_2

The above discussions make it quite obvious that the periodic change in atmospheric pressure has significant role in causing the annual change in CO_2 concentration. Now the pin-pointed investigation is how such change is caused. A conceivable reason may be the transfer of more amount of surface-level CO_2 to higher altitudes thereby increasing the effective average concentration throughout the whole atmospheric path for the absorption of solar radiation. The *El Nino* effect (Keeling et al., 1996; Nevison et al., 2008; Jiang et al., 2013; Ravi Kumar et al., 2016) is a worthy evidence to corroborate such possibility when the warm atmosphere corresponds to the growth of CO_2 flux. The spectroscopic technique for estimating the atmospheric gas concentration from the absorption depth relies on the principle of radiation attenuation through the average gaseous concentration of the total atmospheric path and not that adjacent to the earth surface. The expanding surface-level CO_2 up to higher altitudes, as expected above, may contribute more to the radiation attenuation resulting in a higher effective concentration of CO_2. Such a possibility of apparent increase of CO_2 concentration in established here with the following two independent demonstrations:

- the results of ground-based spectroradiometric measurements and
- the redistribution model for CO_2 concentration developed in Section 6.3.

Table 6.4 presents a set of comparative results on the directly measured local CO_2 concentration at the ground-level and the spectroscopic retrieval of the atmospheric column average of CO_2 concentration at the same site. The places of dense population and high vehicle-congestion have higher ground-level CO_2 concentration, as expected but it is quite interesting to note that these places need not possess always higher column averaged value of CO_2. This result establishes that the local CO_2 concentration at ground level and that averaged over the whole atmospheric column are two different entities. The ground level CO_2 takes a long period to get assimilated uniformly in the air whereas the air-mixed component of CO_2 is subject to instantaneous changes in atmospheric conditions.

Table 6. 4. CO_2 concentration measured at ground level (with GCH-2018 CO_2 meter) and estimated for atmospheric column average (from ASD spectroradiometry) at different types of sites. Climatic conditions: full sun, temperature 33 to 34 °C, humidity 44%, pressure 1007 mbar, wind SW 9 km hr^{-1}.

Ambient condition of the site	Approximate time of measurement	Solar illumination (klux)	Ground-level CO_2 concentration (ppm)	Atmospheric average of CO_2 concentration (ppm)	
				From CO_2-1	From CO_2-2
Less population, less vehicles (suburban area)	09:00 AM	48.0 to 49.2	410 to 412	336 to 337	335 to 336
	10:30 AM	58.0 to 63.0	386	380	390
Dense population, more vehicles (busy road)	11:30 to 11:45 AM	67.2	540 to 542	415 to 417	431 to 432
Car parking lot	12:00 to 12:10 PM	58.0 to 58.2	504 to 505	437 to 438	423 to 424
Grass field of city	01:15 to 01:30 PM	62.0 to 62.5	450 to 453	429 to 431	405 to 406
7^{th} floor rooftop, windy atmosphere	01:30 to 01:45 PM	55.5 to 57.2	390 to 395	400 to 402	412 to 414

The theoretical model for the vertical redistribution developed in section 6.3 quantifies this concept. Figure 6.9 presents several theoretical variations for CO_2 concentration (ppm) generated with equations (6.1), (6.4) and (6.8). These demonstrate the change in CO_2 vertical concentration profile caused by air temperature (solid and dotted lines) and the consequent air pressure with different extents of unmixed vertical transport component [$\upsilon(z)$] and other changed parameters (h, σ and χ) indicated in the figures. The figures explain that the vertical profiles of CO_2 may differ broadly but the phenomenon of vertical redistribution of CO_2 molecules takes place irrespective of the presence of the vertical transport component. The effect is more prominent in the lower atmosphere ($\leq$ 5 km).

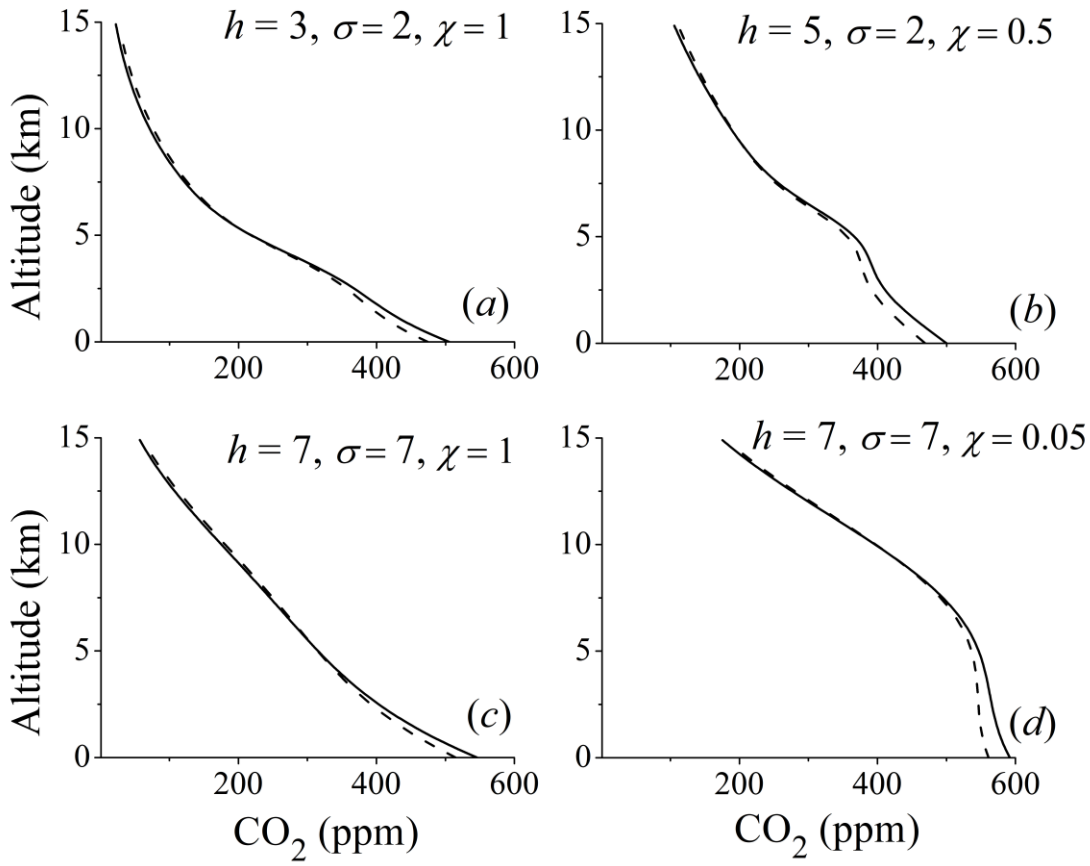

Figure 6. 9. Theoretical curves generated with equations (6.1), (6.4) and (6.8) demonstrating the change in CO_2 vertical concentration profile due to change in air temperature from 300 K (solid line) to 320 K (dashed line) and the consequent air pressure in presence of different extents of vertical transport component: (*a*) 10%, (*b*) 10%, (*c*) 25% and (*d*) 50% of ground level concentration and other changed parameters indicated in the figures.

Now figures 6.2 and 6.7 may be revisited in the light of the above explanation for vertical redistribution of atmospheric CO_2. The figures display a common feature of CO_2 increase in summer. It is understood that in summer seasons, the higher surface temperature causes the surface pressure to decrease. The decreased surface pressure, in turn, expands the surface-level air. Along with the expanding air, the mixed component of CO_2 is carried to higher altitudes thereby expanding the effective length of absorption. This causes more attenuation of radiation through the whole atmospheric path and results

in an enhanced CO_2 concentration. The order of this change may be as large as the order of the observed seasonal changes.

Table 6.5 presents some comparisons of the practical results on the extent of CO_2 seasonal variation with the potential change in CO_2 due to temperature fluctuation predicted by the redistribution model. The validation process is outlined in section 6.3.2. Considering the maximum and minimum CO_2 values equivalent to n_{01} and n_{02}, respectively, of Equation (6.11) and the temperatures equivalent to T_{02} and T_{01} correspondingly, calculations were made for the reduced concentration with increased temperature using Equation (6.11). It is noted that the maximum values come down to almost of the order of the minimum values.

Table 6. 5. Some comparisons of the extent of CO_2 seasonal variation with the possible change due to temperature fluctuation according to Equation (6.11).

Referred data from Figure	CO_2 (ppm)		Corresponding temperature (K)		Reduced CO_2 (ppm) [Equation (6.11)]
	Maximum (n_{01})	Minimum (n_{02})	Maximum (T_{02})	Minimum (T_{01})	
6.2(a): 2017 6.5(c): 2017	406.1	404.3	283.7	282.5	404.4
6.2(b): 2018 6.5(d): 2018	409.2	404.8	284.5	281.6	405.0

Another validation of the model is presented in Figure 6.10. It simulates the annual percentage change in seasonal CO_2 where the CO_2 concentration is generated for each day using the redistribution model (section 6.3). The curves A and B in Figure 6.10 correspond to the vertical profiles of Figure 6.9(*a*) and 6.9(*d*), respectively. The extent of seasonal variation in Figure 6.2 is about 2.5% to 5% so that the simulation in Figure 10 is shown for the same order. Curve-C (dashed line) indicates how the variation would change with annual monotonic increase. Curve-D (dot-dashed line) indicates the nature of variation with both monotonic increase and vegetation uptake.

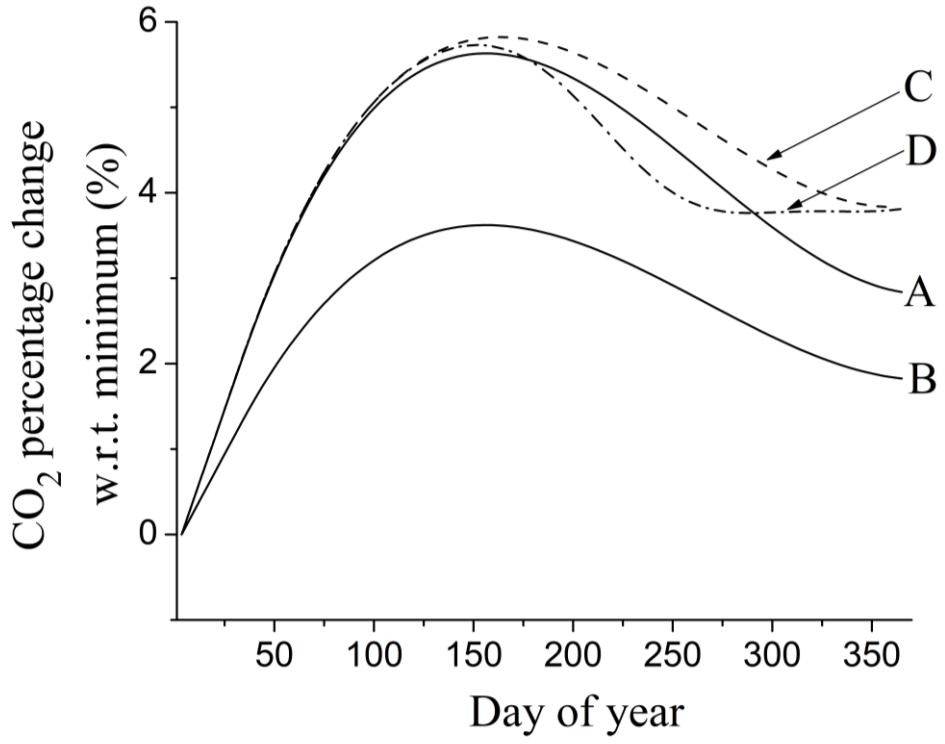

Figure 6.10. Annual percentage change in seasonal CO_2 concentration simulated with Equation (1) for the vertical profiles of Figure 6.9 (*a*) (curve-A) and Figure 6.9 (*d*) (curve-D). The dotted lines indicate the trend of variation with annual monotonic increase (curve-C) and with the combination of monotonic increase and vegetation uptake (curve-D).

The model for vertical redistribution of atmospheric CO_2 molecules under changed condition of temperature and pressure is propounded as an interpretation for the observed seasonal change of CO_2 concentration. The above discussions state that whatever may be the hue of the vertical profile of CO_2, its concentration at an arbitrary height with respect to the concentration at the ground level can change with the variation in temperature and pressure giving rise to an apparent change in effective concentration throughout the path, hence in the spectroscopic results. Since these parameters must be present in some form or other in the climate modelling for global level, a similar seasonal variation can be expected for comparable climates.

6.5. Inferences

This part of the present work investigates the seasonal change of atmospheric CO_2 concentration, identifies the effects of atmospheric pressure and temperature on such change and put forward an illustrative climate model based on vertical redistribution of CO_2 molecules for interpreting such results. The study was initiated at the background of the following three parameters:

- a well observed and known seasonal trend of CO_2,
- a well-accepted explanation of vegetation vigour for the same and
- the mismatch of differed results on the annual variability at different locations with diversified explanations.

The problem was addressed with the following investigations.

(A) Satellite Data Analysis: OCO-2 and NASA-Giovanni data on the trend of CO_2 seasonal change, the corresponding vegetation parameters, namely SIF and NDVI and atmospheric pressure and temperature are evaluated in two steps: high temporal resolution data for a specific region and long-term, coarser resolution data over a larger region, both being part of the tropical, plain area of India. The periodic increase and decrease in the annual trend of CO_2 was tracked with third order polynomial. In order to find out the role of the actual periodicities, the temporal variations were investigated in frequency domain also.

The extent of SIF, a representative of carbon sequestering by photosynthesis matched the periodicity but could not explain the prominent increase of CO_2 during a year. Thus the existence of some other factor was predicted. Since the parameters investigated in the previous reports are somehow related to atmospheric pressure, this quantity and the corresponding temperature values were explored. Several noted features, such as decrease in surface pressure in monsoon/autumn and increase in winter and lowering of pressure during increasing CO_2 indicated a strong influence of atmospheric pressure on CO_2 variation. Both NDVI and atmospheric pressure were found to have a combined

effect on the seasonal variation of CO_2 concentration. Each component of variation was identified with frequency-domain analysis.

(B) Ground measurements: Field studies were conducted to measure the surface-level CO_2 concentrations at places of varying urban congestion and the column averaged CO_2 concentrations at the same places were estimated from absorption spectroscopy. The comparison of these two established the separate existence of the local unmixed and the column averaged air-mixed CO_2 concentrations.

(C) Redistribution Model for CO_2: A mathematical model is developed for vertical redistribution of CO_2 molecules under changed conditions of temperature and pressure, which interprets that the pressure change merely redistributes the vertical arrangement of CO_2 molecules and does not actually remove or introduce any CO_2 molecule. However, this vertical rearrangement of molecules contributes to an apparent change of atmospheric path for radiation absorption. The spectroscopic assessment of gas concentration is based on the extent of radiation absorption, which depends on the number of molecules in the atmospheric path subject to pressure variation. Whether or not the vertical CO_2 profile gets changed due to the diffusion of unmixed components, the number density of air-mixed atmospheric CO_2 at an arbitrary altitude may change with the seasonal alteration of surface air temperature, hence that of the air pressure. This simple model not only explains the present findings, it is also expected to provide with a climate model explaining the atmospheric CO_2 concentration at an arbitrary altitude under the influence of temperature and pressure.

Chapter References

Basu, S., Krol, M., Butz, A., Clerbaux, C., Sawa, Y. & Machida, T. et al. (2014). The seasonal variation of the CO2 flux over Tropical Asia estimated from GOSAT, CONTRAIL, and IASI. *Geophysical Research Letters*, 41(5), 1809-1815. doi: 10.1002/2013gl059105

Berner, R. (2003). The long-term carbon cycle, fossil fuels and atmospheric composition. *Nature*, *426*(6964), 323-326. doi: 10.1038/nature02131

Diallo, M., Legras, B., Ray, E., Engel, A. & Añel, J. A. (2017). Global distribution of CO_2 in the upper troposphere and stratosphere. *Atmospheric Chemistry and Physics*, 17(6), 3861-3878. doi: 10.5194/acp-17-3861-2017

Elachi, C., & Van Zyl, J. (2006). *Introduction to the physics and techniques of remote sensing* (2nd ed.). New Jersey & Canada: John Wiley & Sons, Inc.

Gamon, J. A., Field, C. B., Goulden, M. L., Griffin, K. L., Hartley, A. E. & Joel, G. et al. (1995). Relationships Between NDVI, Canopy Structure, and Photosynthesis in Three Californian Vegetation Types. *Ecological Applications*, 5(1), 28-41. doi: 10.2307/1942049

Jiang, X., Wang, J., Olsen, E. T., Liang, M., Pagano, T. S. & Chen, L. L. et al. (2013). Influence of El Niño on Midtropospheric CO_2 from Atmospheric Infrared Sounder and Model. *Journal of the Atmospheric Sciences*, 70(1), 223-230. doi: 10.1175/jas-d-11-0282.1

Keeling, C., Chin, J., & Whorf, T. (1996). Increased activity of northern vegetation inferred from atmospheric CO_2 measurements. *Nature*, 382(6587), 146-149. doi: 10.1038/382146a0

Nestola, E., Calfapietra, C., Emmerton, C., Wong, C., Thayer, D. & Gamon, J. (2016). Monitoring Grassland Seasonal Carbon Dynamics, by Integrating MODIS NDVI, Proximal Optical Sampling, and Eddy Covariance Measurements. *Remote Sensing*, 8(3), 260. doi: 10.3390/rs8030260

Nevison, C. D., Mahowald, N. M., Doney, S. C., Lima, I. D., van, der Werf G. R. & Randerson, J. T. et al. (2008). Contribution of ocean, fossil fuel, land biosphere, and biomass burning carbon fluxes to seasonal and interannual variability in atmospheric CO_2. *Journal of Geophysical Research: Biogeosciences*, 113(G1), n/a-n/a. doi: 10.1029/2007jg000408

Queißer, M., Burton, M. & Kazahaya, R. (2019). Insights into geological processes with CO_2 remote sensing – A review of technology and applications. *Earth-Science Reviews*, 188389-426. doi: 10.1016/j.earscirev.2018.11.016

Ravi Kumar, K., Tiwari, Y., Revadekar, J., Vellore, R., & Guha, T. (2016). Impact of ENSO on variability of AIRS retrieved CO_2 over India. *Atmospheric Environment*, 142, 83-92. doi: 10.1016/j.atmosenv.2016.07.001

Sawyer, J. (1972). Man-made Carbon Dioxide and the "Greenhouse" Effect. *Nature*, *239*(5366), 23-26. doi: 10.1038/239023a0

Stockie, J. M. (2011). The Mathematics of Atmospheric Dispersion Modeling. *SIAM Review*, 53(2), 349-372. doi: 10.1137/10080991x